Cite this: *Soft Matter*, 2011, **7**, 3947

www.rsc.org/softmatter

PAPER

Investigations of vesicle gels by pulsed and modulated gradient NMR diffusion techniques

Samo Lasič,*[ab] Ingrid Åslund,[a] Claudia Oppel,[c] Daniel Topgaard,[a] Olle Söderman[a] and Michael Gradzielski[c]

Received 8th November 2010, Accepted 28th January 2011
DOI: 10.1039/c0sm01278e

Vesicle gels are surfactant systems that form stiff gels with rather low amounts of surfactant. So far their structures have mostly been investigated using scattering techniques, which are generally appropriate for the study of structures on the nm-length-scale. Here we examine these gels using two complementary diffusion NMR techniques, which are both sensitive to structures on the μm-scale. The presented results imply structural features on the μm-scale, indicating a more complex structure than just that of densely packed small vesicles, as previously found for these systems. It is demonstrated that a combination of the diffusion NMR methods, described here, can provide useful insights, when morphological features extend over a wide range of length scales.

1 Introduction

A multitude of different structures can be obtained from self-assembled surfactant and block copolymer systems, including micelles and liquid crystals.[1–4] An important class of structures formed are constituted by bilayers and vesicles, *i.e.* spherically closed bilayers. Such vesicles may occur as unilamellar or multilamellar vesicles.[5] They can be used in diverse applications, such as formulations for softeners, nanoreactors, material templates and cell membrane models. They are also interesting for a fundamental understanding of molecular and colloidal interactions and for being model systems for membranes.

For sufficiently high concentrations of surfactants, vesicles will be densely packed and this will lead to a substantial increase in viscosity and even to the formation of vesicle gels, *i.e.* systems that posses a yield stress. Such behaviour has for instance been observed for densely packed multilamellar vesicles.[5–7] However, it has also been observed that unilamellar vesicles composed of anionic surfactant, cosurfactant, and water can form such a vesicle gel spontaneously. These systems are viscous and according to previous experimental investigations they consist of monodisperse unilamellar small vesicles with a radius of about 15–25 nm.[8–11] The fact that they are unilamellar and relatively small, is rather uncommon for spontaneously forming structures, *i.e.* their formation must be driven by the spontaneous curvature of the bilayer due to an asymmetry induced by the mixture of surfactant and cosurfactant.

[a]*Division of Physical Chemistry, Center of Chemistry and Chemical Engineering, Lund University, Lund, Sweden*
[b]*Colloidal Resource AB, Kemicentrum, Box 124, 221 00 Lund, Sweden. E-mail: samo.lasic@fkem1.lu.se; Tel: +46 222 94 80*
[c]*Stranski-Laboratorium für Physikalische Chemie und Theoretische Chemie, Institut für Chemie, Technische Universität Berlin, Berlin, Germany*

Earlier works have generally focused on scattering techniques along with electron microscopy and conductivity measurements.[5,8–10] In this work the focus is on nuclear magnetic resonance (NMR). Here two diffusion NMR techniques are used to examine the structure, *viz.* the pulsed-field-gradient spin-echo (PGSE) and the modulated gradient spin-echo (MGSE) techniques.[12]

Diffusion NMR techniques can detect different features of the diffusion process.[12,13] Since diffusion is affected by the sample morphology, structural information can be obtained. With the available experimental equipment to date, such techniques can probe structures typically down to the micrometer length scale.

In the PGSE approach a pair of short magnetic field gradient pulses is used to label the start and the end positions of molecular diffusive paths during the interval between the two pulses to yield the molecular mean square displacement. In fact, this is only true if molecular displacements during the application of the pulses are shorter then the characteristic size of the restrictions present in the sample.[14] This condition is generally known as the short-gradient-pulse (SGP) approximation.

Kärger and Heink[15] realized that the PGSE experiment can be used to probe the Fourier representation of the real space average displacement propagator. Callaghan *et al.*[16–18] used the q-space as a structure analysis concept in PGSE experiments, when the SGP approximation is fulfilled. The parameter q is the wave vector along the applied magnetic field gradient and is determined by the strength and duration of the gradient pulses. Since the average displacement propagator is related to the position dependent spin density, which reflects geometrical features of materials, q-space imaging[16] is similar to scattering techniques.[12] Diffraction-like effects in the echo attenuations result when q-space imaging is applied to locally ordered structures.[18]

Due to instrumental limitations, it is often difficult to fulfil the SGP condition.[19,20] The effects of the finite duration of the gradient pulses have been experimentally investigated[21,22] and turned into an advantage to probe the intracellular fraction[22] and diffusion coefficient of water in cell suspensions.[23] The variable pulse duration can be used to determine the minimum length-scale at which the diffusion appears Gaussian. For this purpose, the concept of the homogeneous length scale, λ_{hom}, has been introduced in PGSE experiments and applied to determine the characteristic domain size of a micro-heterogeneous lamellar liquid crystal system.[24] For distances shorter than λ_{hom} the sample appears inhomogeneous, which could be caused by either anisotropic domains[24] or restricting confinements.[25] For distances longer than λ_{hom} the structural features are blurred out and the structural information is lost. The PGSE protocol[24] for determining the λ_{hom} was used in this study.

The characterization of diffusion by the PGSE experiment can be complemented and extended by the MGSE approach.[26–29] By generating a periodically oscillating effective magnetic field gradient, the MGSE experiment provides information about diffusion in the frequency domain. The result of the experiment is the signal attenuation, which is proportional to the spectrum of the velocity auto-correlation function (VCF) of the spin-bearing particles. The effect of spin de-phasing, due to diffusion, is accumulated over many gradient modulation cycles, which results in stronger diffusive attenuation on a shorter time scale compared to the conventional PGSE method. The VCF spectrum, also known as the diffusion spectrum, $D(\omega)$, probed by the MGSE approach, is related to the mean square displacement which contains information about the sample morphology.[30] The zero frequency component of the diffusion spectrum corresponds to long range diffusion, while higher frequency components approach the bulk diffusion value. The MGSE approach is able to separate the effects of restricted diffusion from molecular migration across the interconnected porous structure.[31–33] This fact allows one to determine tortuosity as well as the size of restrictions experienced by the diffusing molecules. Different gradient modulation schemes have been employed in MGSE experiments to study water diffusion in porous media[32] and in emulsions.[34]

Here we apply a MGSE method which uses sinusoidal gradient pulses separated by 180° radio frequency (RF) pulses.[33] Such an experiment can be used to determine polydispersity in highly concentrated emulsions on length-scales below μm. Furthermore, it has been shown that MGSE can yield complementary morphological information, as compared to the results of the PGSE experiments applied to the same kind of system.[21]

The above described methods were applied to a system composed of densely packed vesicles. The vesicles are formed in the sodium oleate/octanol/water system, with concentrations of ≈ 0.2 M sodium oleate and ≈ 0.6 M octanol.[9] A sample containing tetramethylammonium as a counterion was also examined in order to obtain results from the (proton containing) counterions. The vesicles are densely packed with a volume fraction of about 0.5.

The aim of this study was two-fold. Firstly, we wish to demonstrate how the novel diffusion NMR methods described above can be used to obtain morphological information for complex soft matter on the micrometer length scale. Secondly, we seek to further characterize the structure of the vesicle gels, in particular on the micrometer length-scale; a length scale which is difficult to investigate by alternative methods. By applying these novel NMR methods we are able to deduce larger scale structural information about the investigated systems.

2 Theory

Diffusion is characterized through the attenuation of signal intensities measured in NMR spin-echo experiments. If there is no net flow and the relaxation is factored out, the normalized echo intensity E can be expressed by the Stejskal–Tanner equation.[35] The expression for the echo intensity can be extended to include contributions from spins with different diffusion properties k

$$E = \sum_k E_k \, e^{-\beta_k}, \tag{1}$$

where $\sum_k E_k = 1$.

The attenuation β_k is proportional to the measured diffusion coefficient D_k

$$\beta_k = bD_k, \tag{2}$$

where the diffusion weighting factor b depends on the effective magnetic field gradient waveform. When diffusion is measured in a porous medium, the D_k values do not necessarily correspond to the bulk diffusion value. If the structure hindrance or confinements affect the spin trajectory during the measurement time, the D_k values will be smaller then the bulk value.[36] In case of microscopically heterogeneous samples, the echo attenuation might be multi-exponential (see eqn (1)) even when spins have a uniform bulk diffusion coefficient. This is due to an occurrence of different sub-ensembles of spins experiencing different morphological features. One example is when morphologically different parts of a sample are separated by distances larger then the spins can diffuse during the experiment. However, a situation characteristic for both the PGSE and the MGSE approaches described here, is the fact that the echo attenuation is given by contributions from different sub-ensembles of spins with different diffusion properties even when the spins can migrate over all the characteristic restrictions during the experimental time. The weighting of the contributions depends on the experimental conditions. Note that due to the low gradient strengths, the MGSE echo decays are mono-exponential, yet given by a weighted average over several sub-ensemble contributions (see section 2.2).

In the limits of very long and very short diffusion times, diffusion can be considered a Gaussian process,[37] while at intermediate times, correlations in the spin trajectory due to restrictions are apparent and diffusion is a non-Gaussian process. At longer diffusion times D_k yields the so-called long range diffusion coefficient D_∞, while at shorter times it approaches the free diffusion value in bulk D_0. The ratio D_0/D_∞ is known as the tortuosity, which is related to the connectivity in the porous sample.

2.1 Pulsed-field-gradient experiments

In the PGSE experiment used in this study, long diffusion times were used to allow the spins migrating over all characteristic

length scales present in the sample.[24] The magnetic field gradient strength g and the pulse duration δ were varied. These two parameters determine the sensitivity to diffusion and define the wave number q as

$$q = \frac{\gamma \delta g}{2\pi}, \tag{3}$$

where γ is the gyromagnetic ratio. The parameter q sets the inverse length scale at which the spin displacements are detected. At low q, *i.e.* low diffusion sensitivity, only large displacements can be detected, while at large q the increased sensitivity allows the detection of smaller displacements.

For the PGSE experiment the parameter b is calculated according to

$$b = (2\pi q)^2 t_d, \tag{4}$$

where t_d is the effective diffusion time, *i.e.* the time between the start of the two gradient pulses Δ reduced by a correction term, which depends on the shape of the gradient pulses.[38,39]

By combining the eqn (3) and (4), it is evident that in the PGSE experiment the echo attenuation in eqn (2) is proportional to the product $D_k t_d$, which is related to the mean square displacement (MSD) along the applied gradient

$$\langle Z_k^2 \rangle = 2 D_k t_d. \tag{5}$$

When diffusion is unrestricted or at diffusion times so short that the probability for spins to meet the confinement is negligible, the D_k values do not depend on time and the echo attenuation is proportional to t_d. At intermediate times, when the confinements significantly affect the diffusion, a decrease of D_k values is observed at increasing t_d. At long diffusion times, when all the spins are affected by the confinement, the echo attenuation becomes independent of t_d, if the pores are closed. In such a case, a time independent MSD value is reached, which depends on the confinement shape and size as well as on the gradient pulse duration.[40] The maximum MSD is observed in the SGP limit. Since the spins are labelled for a position given by the center-of-mass average of their path during the application of the gradient pulse, increasing δ results in position averaging and consequently in a decrease of the MSD and of the echo attenuation.[21,23]

When the PGSE echo decay is probed for a semi-permeable structure and long diffusion times are used, the information extracted from the echo decay depends on the q-value range (see Fig. 3 and Fig. 4). In the range of low q values, where only large displacements contribute to the echo decay, a Gaussian character is retrieved. In this regime, the influence of the structural boundaries has a negligible effect on the position labelled during the application of the pulse and consequently the echo decay at a given q does not depend on δ. Since the structural features cannot be detected at low q values, the sample appears homogeneous. At increasing q values smaller displacements contribute to the echo decay, and the influence of the boundaries on the labelled spin position cause the echo decay to depend on δ.[21] At large q values, corresponding to short length scales, the sample appears inhomogeneous. The q-value at which the echo decay goes from being independent to dependent of δ defines the inverse of λ_{hom}.

When performing a λ_{hom} analysis, it is important to make sure that t_d is sufficiently long so that the spins have passed through enough of the sample during the diffusion time to probe all of its representative parts. To verify this, one needs to examine the initial slope, *i.e.* the low b (or q) values, of the echo attenuations. This part of the data contains information about D_∞, which should be independent of t_d for long times. In one dimension, the corresponding square-root of the long range MSD is given by

$$\langle Z \rangle_{rms} = \sqrt{2 D_\infty t_d}. \tag{6}$$

For restricted diffusion, a previous study shows that λ_{hom} is directly proportional to the length of the periodicity of a micro-heterogeneous medium. Based on the simulations by Åslund *et al.*[25] and assuming spherical restrictions, the characteristic radius of restrictions in given as $\lambda_{hom}/6$.

We stress that the λ_{hom} analysis is a model free way of estimating the range for the characteristic sizes in the system. The value obtained should be considered as a length scale at which there is a cross-over from locally anisotropic to globally isotropic diffusion.[24,25]

2.2 Modulated gradient spin-echo

As in the homogeneous length scale experiment described above, the MGSE experiment also presumes that all the characteristic diffusive modes are observed during the relevant experimental time t_e. The MGSE approach is complementary to the PGSE experiment in several ways. While the PGSE protocol for determining the λ_{hom} monitors diffusion on different length scales, the MGSE approach detects diffusion modes at different frequencies. While the PGSE experiment can accurately determine the long-range diffusion, the MGSE approach probes diffusion on much shorter time scales and is therefore more sensitive to structural features on smaller length scales. In summary, the MGSE operates in the range of small q values. Here, the signal attenuation can be approximated by the second order term in the cumulant expansion, known as the Gaussian approximation.[41] The signal attenuation for the k-th species is given by

$$\beta_k = \frac{1}{\pi} \int_0^\infty |F(\omega)|^2 D_k(\omega) d\omega. \tag{7}$$

where $F(\omega)$ is the spectrum of the phase factor $F(t) = \gamma \int_0^t G(t') dt'$, which is determined by the effective gradient waveform $G(t)$, and $D_k(\omega)$ is the spectrum of the VCF or the diffusion spectrum in the direction along the applied gradient.[26–30] While the PGSE method uses a single pair of spin labelling and de-labelling gradient pulses, the spin-labelling and de-labelling is repeated several times within the MGSE experiment. Thus, adequate signal attenuation can be achieved by using much lower gradient field strength compared to the PGSE approach. This is an essential feature of the MGSE experiment. It means that the spin phase grating, which is inversely proportional to the amplitude of the phase factor, can always be made larger than the size of the confinements under investigation. Thus, the signal intensity of the MGSE experiment can be analyzed within the Gaussian approximation of the cumulant expansion.[42]

The method relies on the rate of the gradient modulation rather than on its magnitude.

If the spectrum of the phase factor $F(\omega)$ has a narrow frequency peak at a non-zero frequency ω_m, the component of the diffusion spectrum at ω_m can be measured. This is achieved by an appropriate choice of the gradient modulation waveform. The pulse sequence used here (presented in Fig. 1) consists of the Carr–Purcell–Meiboom–Gill (CPMG) RF train with $2N$ refocusing 180° pulses and interleaved gradient pulses with sinusoidal shape. The time of echo acquisition is given by $t_e = NT_m$, where N is the number of modulation periods and T_m is the modulation period. The refocusing pulses are separated by $T_m/2$. The shape of the gradient pulses is defined by $g\sin(\omega_m t)$, where $\omega_m = 2\pi/T_m$ is the modulation frequency. Note that the first and the last pulse in the sequence oscillate twice as fast as the rest of the pulses. The corresponding effective gradient $G(t)$ has an apodized cosine shape and the phase factor oscillates periodically around zero with the modulation period T_m. The spectrum of the phase factor $F(\omega)$ has a peak centered around ω_m with a width inversely proportional to t_e. When several modulation periods are applied, the echo attenuation is proportional to the spectral component of the diffusion spectrum at the modulation frequency. It can be expressed in a form similar to eqn (2), as

$$\beta_k \approx bD_k(\omega_m), \tag{8}$$

where b is the attenuation factor. For the pulse train in Fig. 1, b is given by

$$b = \left(\frac{\gamma g}{8\pi}\right)^2 t_e^3 \frac{8N-1}{N^3}. \tag{9}$$

In order to factor out relaxation effects, while probing the diffusion spectrum, the number of modulation periods N is adjusted along with the period T_m providing a constant $t_e = NT_m$. The lowest value of ω_m at which the diffusion spectrum can be probed is limited by the longest t_e value that the T_2 relaxation rate allows, while the upper limit is set by hardware restrictions.

The model for the restricted diffusion spectrum $D(\omega)$ can be analytically derived in cases of simple geometries (planar, cylindrical and spherical).[30] Complex systems often consist of interconnected restricted environments or permeable pores, which define the long-range diffusivity D_∞. This is reflected in the diffusion spectrum as a finite component at zero frequency. Assuming that the long-range diffusion mode is probed during t_e, the expression for $D(\omega)$ can be extended by an additional tortuosity term as

$$D(\omega) = \alpha D_0 + (1-\alpha)D_0 \sum_{k=1}^{\infty} \frac{a_k B_k \omega^2}{a_k^2 D_0^2 + \omega^2}, \tag{10}$$

where $\alpha = D_\infty/D_0$ is the inverse tortuosity. The coefficients a_k and B_k depend on the geometry under consideration.[30,33] As a rough model of our system we assume restrictions of spherical geometry. For a pore radius R, the coefficients a_k and B_k are given by

$$a_k = \left(\frac{\zeta_k}{R}\right)^2 \tag{11a}$$

$$B_k = \frac{2(R/\zeta_k)^2}{\zeta_k^2 - 2}, \tag{11b}$$

where ζ_k are kernels of

$$\mu J_{1/2}(\zeta) - 2J_{3/2}(\zeta) = 0 \tag{12}$$

and J_ν denotes ν-th order Bessel function of the first kind.

For the case of polydispersity in restriction sizes, the echo decay would generally be multi-exponential (see eqn (1)). However, if the molecules can migrate between regions with different morphology, so that they experience all characteristic restrictions in the sample during the MGSE experiment, the echo decay is mono-exponential and determined by the average diffusion spectrum $\bar{D}(\omega_m, \alpha)$, which is given by the volume weighted sum over sub-ensembles of spins originating in regions of the sample with different restrictions[33]

$$\bar{D}(\omega_m, \alpha) = \sum_R P(R) D(R, \omega_m, \alpha). \tag{13}$$

2.3 Diffusion in vesicles

In vesicle systems, three regions with different diffusive properties can be identified. The first region is the interior of the vesicle. The second region is the membrane or shell of the vesicle. The effect the membrane has on the diffusion depends on both the solubility of the molecules in the membrane and on the diffusion of the molecules inside the membrane. The third region is the continuous surrounding media. It should be noted that the dense packing of the vesicles imposes restrictions on the diffusion also in this region.

In these types of systems with different regions the measured diffusion coefficient depends on the time-scale of the experiment and the time-scale of the molecular exchange between the different regions. If the exchange time is long compared to the experimental time-scale, the measured signal will be a superposition of the signal from the different regions and eqn (1) can be used. If, on the other hand, the exchange time is shorter than the measuring time-scale the signal attenuation is given by the

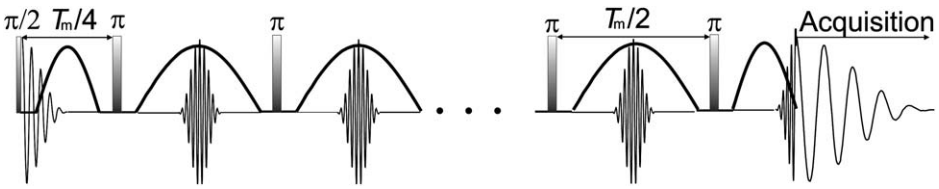

Fig. 1 Schematic timing of the RF pulse sequence with sinusoidal gradient lobes. An even number of the refocusing pulses is used, separated by $T_m/2$.

time-averaged signal of diffusivity in the different regions. Such is the case in the MGSE experiment (see eqn (13)).

The exchange time τ for migration of water molecules between the internal vesicular space and the surrounding can be estimated with appropriate assumptions. For a spherical vesicle, the relation between the membrane permeability P, the vesicle radius r and the exchange rate $k = 1/\tau$ is[43]

$$P = k\frac{r}{3} \Rightarrow \tau = \frac{r}{3P}. \quad (14)$$

For the vesicles used in this work a radius of $\approx$20 nm has been deduced using neutron scattering data.[5] The permeability of bilayers is generally within 2–100 μm s^{-1} for water.[1] This would suggest an exchange time of 0.07–3 ms for the present system.

In the diffusion-NMR experiments the time scale of the measurement is typically between 1 ms and a few 1 s, depending on sample, technique and instrument. Thus, if only small vesicles are present any structural information related to the vesicles should be averaged out and not be measurable with the NMR techniques.

The long-range diffusion coefficient D_∞ can be estimated using the cell model approach for a spherical region 1 being surrounded by a region 2:[44]

$$D_\infty = D_2 \frac{1}{1-\left(1-\frac{C_1}{C_2}\right)\Phi} \frac{1-\theta\Phi}{1+\frac{\theta\Phi}{2}} \quad (15)$$

where

$$\theta = \frac{D_2C_2 - D_1C_1}{D_2C_2 + \frac{D_1C_1}{2}}. \quad (16)$$

D_i is the diffusion coefficient for the molecules in region i, C_i is the concentration in region i and Φ is the volume fraction of the enclosed region 1. Note that this model is only valid if the diffusion of vesicles during the experiment can be considered negligible.

The diffusion properties in the vesicle gels can be obtained by using the model in two steps. First, one calculates D_∞ for the vesicle, with region 1 being the inner core and region 2 being the surrounding bilayer. In the next step one calculates D_∞ for the entire system by using the obtained D_∞ from the first step and a calculated mean concentration for the vesicle (including the interior and the enclosing bilayer) as region 1 and the surrounding medium (the continuous water region) as region 2. For reasonable values for the different parameters using water[45] (including an obstruction factor for the diffusion coefficient of the surrounding water) a value of D_∞ of $\approx 1 \times 10^{-9}$ m^2 s^{-1} is obtained, not much different than the bulk diffusion coefficient of water (2.3×10^{-9} m^2 s^{-1}).

3 Experimental

3.1 Sample

The two samples used in this study are identical except for the type of surfactant counterion. They are made from a stock solution of 200 mM cation-oleate in a mixture of H_2O and D_2O (20 : 80), in order to adjust the concentration of H_2O so that in the NMR experiments one can follow the diffusion of water, surfactant, and counterion independently. The cation is either tetrametylammonium (TMA^+) or sodium (Na^+). The stock solution has then been mixed with 1-octanol to a final concentration of 7.5 wt-%.

3.2 NMR experiments

The experiments were performed at 25 °C on a Bruker AVII-200 spectrometer at 200.13 MHz proton resonance frequency. Gradients where generated by a Bruker DIFF-25 probe controlled by a Bruker GREAT 1/40 gradient amplifier with a maximum gradient strength of 9.6 T/m in the z-direction.

For the PGSE-experiments a stimulated echo sequence was used.[46] During the experiments both δ and t_d were varied. Four different values for t_d were used (logarithmically spaced between 30.1 and 200 ms), while δ was logarithmically spaced between 2 and 20 ms in 4 steps. The set of q-values was kept constant by adjusting the gradient strength as δ was changed. For the smallest value of δ, the gradient strength was logarithmically spaced between 1 and 100% of the maximum value possible.

The MGSE experiment was performed with constant t_e = 100 ms. Diffusion was probed at 8 different modulation frequencies. The numbers of modulation periods N were between 10 and 45 incremented by 5. This corresponds to 8 modulation periods T_m between 2.2 ms and 10 ms. The gradient amplitude was adjusted so that the same 16 linearly stepped b values were applied at each modulation period. The maximum gradient amplitude used at the shortest value of T_m was 3.51 T m^{-1}. The standard 8 steps CPMG phase cycling was applied.

3.3 SANS experiments

The SANS measurements were performed at the Laboratoire Léon Brillouin, Saclay (France), on the instrument PAXE. A wavelength of 0.5 nm (FWHM 10%) was chosen, and a fixed sample to detector distance of 5 m was used, with the detector off-center. All samples were measured in 1 mm thick rectangular quartz cells. The data were recorded on a 64 × 64 cm^2 two-dimensional detector. The data reduction was done by the program BerSANS.[47] Data were corrected for detector background, the scattering of the empty cell, radially averaged and converted into absolute units using the direct beam flux.

Sample volumes of about 1 mL were prepared by weighing in first stock solutions of Na- and/or TMA-oleate in D_2O and then an appropriate amount of 1-octanol. Homogenization was done by vigorous shaking with a Vortex for about 15 s. Afterwards the mixed components were immediately transferred into quartz cuvettes (Hellma), while still being relatively low viscous. Samples were aged in cuvettes about one and a half day before being measured.

4 Results and discussion

This section is organized as follows. We start by giving some introductory remarks, followed by the short account on the SANS data. We then proceed to describe and discuss the results from the PGSE and MGSE experiments. A short summarizing discussion is given in the end of this section.

As an introductory remark, we note that in both the PGSE and the MGSE experiments the surfactant/cosurfactant peaks show

such a small attenuation and low signal-to-noise ratio, caused by both low concentration and relaxation effects, that no quantitative conclusions can be made. However, a slight diffusive attenuation of these peaks can be observed (not shown here). This indicates a very slow diffusion of the surfactant and/or co-surfactant molecules. These peaks will not be discussed further and throughout the text concerning NMR below focus will be on the water and TMA peaks.

4.1 SANS measurements

To investigate whether the type of counterion influences the morphology of the vesicle gels SANS measurements were carried out. Two otherwise identical vesicle gel systems with Na^+ or TMA^+ as counterions were examined. Scattering curves of these systems are shown in Fig. 2. The total composition of the investigated samples correspond with the ones used in the NMR studies. In the SANS experiments the surfactant was varied systematically from pure Na oleate over the corresponding mixtures to pure TMA oleate in D_2O. The scattering curves of the vesicle gels are similar for both the pure and the mixed counterion samples. Accordingly, the structural ordering, that is manifested in the q-range from 0.2 to 0.5 nm^{-1}, is very similar. In addition, the large q-behaviour is almost identical for all the samples, which means that their local bilayer structure is similar, with a bilayer thickness of around 2.2 nm. In summary, the vesicle gels possess a similar structural organisation for the different counterions. Thus the comparison of the NMR results for these samples is reliable.

4.2 λ_{hom} Measurements

From the D_∞ values presented in Table 1 it can be concluded that the long-range diffusion regime was reached for water. On the other hand, one should take care when interpreting the results for TMA, which can not be confirmed to reach the long-range limit.

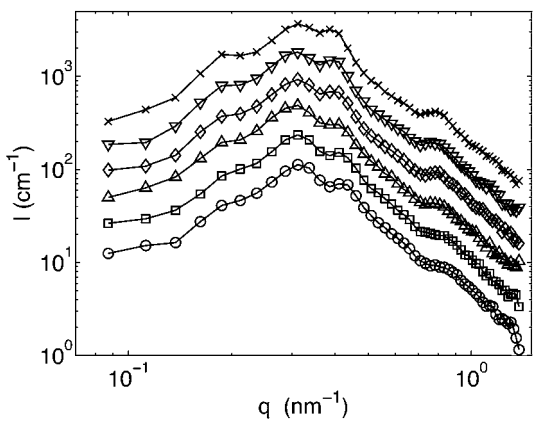

Fig. 2 SANS curves of the vesicle gel samples with gradual exchange of TMA-oleate for Na-oleate at 25 °C, taken at about one and a half days after preparation. The different TMA/Na-ratios are shown with different symbols: 0/100 (circles), 20.3/79. 7 (squares), 40.6/59.4 (triangles up), 59.7/40.3 (diamonds), 79.5/20.5 (triangles down) and 100/0 (crosses). For clarity the intensities starting from the second curve in the plots are multiplied by a consecutive factor of 2.

It is not surprising that the different compounds reach the long-range regime at different diffusion times. In fact, they are expected to reach the long-time regime at a the same Z_{rms}. One reason is the difference in the bulk diffusion coefficient (see the MGSE results) and another is the difference in solubility in the bilayer (the ions can be expected to have a very low solubility in the non-polar bilayer while the water molecules have a slight solubility).[21,33] The values of D_∞ presented in Table 1 are lower by roughly a factor of 2 than the estimation given in section 2.3. We will return to this fact below.

The shape of the decays are presented in Fig. 3 and 4, clearly showing more than one exponential component, indicating the presence of larger confinements hindering the diffusion. In these figures the echo attenuations for two of the different t_d and for all four different δ values are presented. The data for the TMA-oleate sample are presented in Fig. 3, while the data for the Na-oleate sample can be found in Fig. 4.

The λ_{hom} is obtained as an inverse of the q value at which the relative difference between the signal intensities for the longest and the shortest δ at a constant t_d reach a certain threshold value.[24] Because of the concentration and attenuation differences, the different species were assigned different threshold values to define a deviation (10% for the water peak and 2% for the TMA-peak). The λ_{hom} is only well defined for long-range diffusion and thus the data at the longest t_d is used to determine it. The threshold is reached at a q value of about 4×10^4 m^{-1}, which is similar for both species (water and ion) and both samples, as indicated by the vertical lines in Fig. 3 and 4, along with the values given in Table 2. This indicates a λ_{hom} of about 25 μm, and thus a restriction radius of about 4 μm (see section 2.1).

The water peak for the Na-oleate system appears to have a more distinct biexponential decay. This would indicate a longer exchange time between the compartments, as discussed in the theory. The increase in exchange time could be caused by, for example, increase in restriction size and/or decrease in permeability (see eqn (14)).

4.3 Diffusion spectrum measurements

The intensities of the water and TMA peaks were analyzed in terms of Stejskal-Tanner plots, which reveal mono-exponential decays (not shown here). Exponential fits on the graphs of echo intensities E *vs.* b at different T_m give the diffusion spectra results, shown in Fig. 5 and 6.

The mono-exponential decays observed by the MGSE experiments indicate that different morphological regions are connected, so that the molecules can migrate between them during the experimental time t_e (see the Theory section). This is consistent with the large long-range diffusion values obtained from the PGSE experiments and confirmed by the MGSE experiments (see Table 1). Therefore the analysis in terms of eqn (13) can be used to describe the measured $D(\omega)$ data.

The single-size model cannot be fitted to the diffusion spectra shown in Fig. 5 and 6. Instead eqn (13) is fitted to the data by tentatively assuming a log-normal volume-weighted size distribution of restrictions with spherical geometry. Such a choice of the size distribution is justified as it is commonly used to describe

Table 1 The obtained D_∞ and Z_{rms} using the initial slope of the echo attenuations and eqn (1) and 6 for the PGSE experiments for different values of t_d. For each t_d value, an average is calculated for the different δ values used. For comparison the values obtained from the MGSE experiments by extrapolation to zero frequency are given

	t_d (ms)	30.1	56.6	106	200	MGSE
H_2O in	D_∞ (10^{-10} m^2 s^{-1})	4.7	4.7	4.5	4.2	4.6
TMA-oleate	Z_{rms} (μm)	5.3	7.3	9.8	13	
TMA^+ in	D_∞ (10^{-10} m^2 s^{-1})	1.2	1.1	0.96	0.79	0.73
TMA-oleate	Z_{rms} (μm)	2.7	3.6	4.5	5.6	
H_2O in	D_∞ (10^{-10} m^2 s^{-1})	4.0	4.4	4.5	4.5	4.5
Na-oleate	Z_{rms} (μm)	4.9	7.0	9.8	13	

size polydispersity.[48–50] The probability density of a log-normal distribution is given by

$$P(R) = \frac{1}{\sqrt{2\pi}sR}\exp\left[-\frac{(\ln R - \ln R_0)^2}{2s^2}\right], \quad (17)$$

where R_0 is the median and s is the standard deviation of $\ln R$. The mean value is provided by $\langle R\rangle = R_0 e^{s^2/2}$.

The bulk diffusion values D_0 used in the model (10) are assumed to be 2.0×10^{-9} m^2 s^{-1} for water (or rather a mixture of H_2O/D_2O of 20/80) and 1×10^{-9} m^2 s^{-1} for TMA.[33] The size distribution is represented by 100 linearly spaced bins between 1 nm and 50 μm. In the case of TMA-oleate both water and TMA data are well described by a common size distribution of spherical restrictions (Fig. 5). It should be noted that a fit of reasonable quality is obtained only if the two inverse tortuosities α are allowed to be different for the water and TMA data. This is likely due to different membrane permeabilities for water and salt. A global fit yields volume-weighted distribution parameters $R_0 = 0.4$ μm and $s = 1.9$ and inverse tortuosities of $\alpha = 20\%$ for water and 7.3% for TMA.

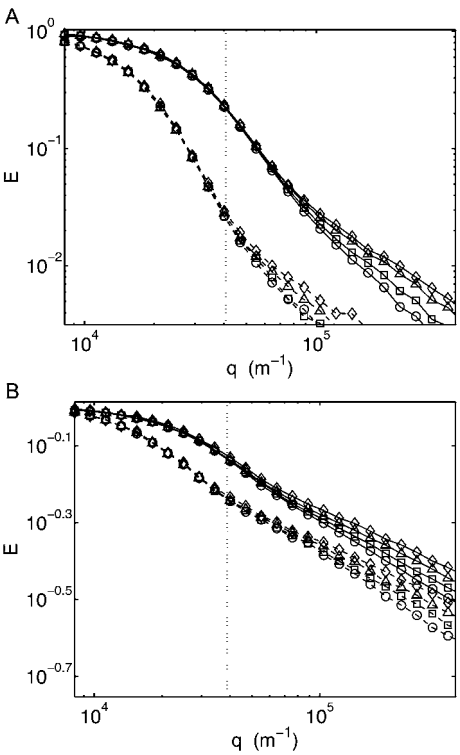

Fig. 3 The normalized echo attenuations for the water peak (A) and the TMA peak (B) for the TMA-oleate system. For clarity only two of the used t_d values are shown. The different line types (which are included to guide the eye and for identification) indicate the value of t_d used (56.7 ms = solid and 200 ms = dashed). The markers indicate different δ values; 2.0 ms (circles), 4.3 ms (squares), 9.8 ms (triangles) and 20 ms (diamonds). The vertical dashed line indicates the inverse of λ_{hom} for the longest t_d. Note the different scales of the ordinate axis for the two graphs.

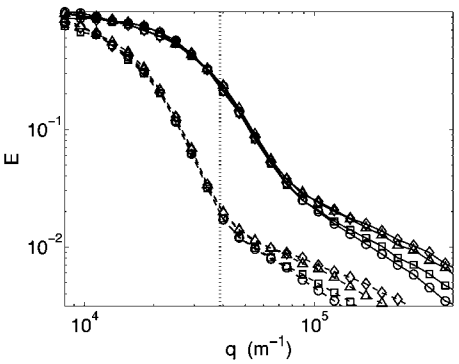

Fig. 4 The echo attenuations for the water peak in the Na-oleate vesicle gel. For clearness only two of the used t_d values are shown. The different line types indicate different values of t_d used (56.7 ms = solid and 200 ms = dashed). The markers indicate different δ values; 2.0 ms (circles), 4.3 ms (squares), 9.8 ms (triangles) and 20 ms (diamonds). The vertical dashed line indicates the inverse of λ_{hom} for the longest t_d.

A large value of s means that the size distribution has a long tail. Even though the general restriction size is in the nm-range there are a few but much larger restrictions (in the range of 10 μm) present in the sample. Both the PGSE and MGSE diffusion experiments are sensitive to these larger restrictions, because of volume-weighting effects.

In the case of the TMA-oleate system the size distribution parameters correspond to a mean restriction size of approximately $\langle R\rangle = 2.4$ μm. The inverse tortuosity values give the long-range diffusion coefficients (see eqn (10)) which are in good agreement with the values observed by the PGSE method. These can be estimated from the attenuation of the echo intensities in the limit of low b values (see Table 1). The small differences of D_∞ between the PGSE and MGSE experiments are most likely due to the fact that the long-time limit has not been reached, particularly in the case of TMA, as discussed above.

In the case of the Na-oleate system, the water data (Fig. 6) was fitted by the two size distribution parameters, while α was fixed to the value of 19.6%, which was obtained from the PGSE results (see Table 1). The resulting distribution parameters are $R_0 = 0.2$ μm and $s = 2$ corresponding to the mean size of approximately 1.5 μm. The sizes obtained from the PGSE and the MGSE methods respectively are summarized in the Table 2.

In summary, both diffusion methods reveal confinements, which are polydisperse in size and on the μm length scale. The results from the MGSE experiments suggest that most of the confinements are below μm in size. However, a small fraction of confinements in the range of 10 μm-scale suffices to account for the restricted diffusion effects observed by both methods. We stress that these results do not exclude the occurrence of

Table 2 Summary of the sizes obtained from the PGSE (λ_{hom}, the characteristic radius of restriction $\lambda_{hom}/6$, see text for details) and the MGSE (R_0, s, $\langle R \rangle$) experiments for the systems with TMA-oleate and Na-oleate. The meaning of the symbols is described in the text

	λ_{hom} (μm)	$\lambda_{hom}/6$ (μm)	R_0 (μm)	s	$\langle R \rangle$ (μm)
H_2O in TMA-oleate	25	4.2	0.4	1.9	2.4
TMA^+ in TMA-oleate	26	4.3	0.4	1.9	2.4
H_2O in Na-oleate	25	4.2	0.2	2	1.5

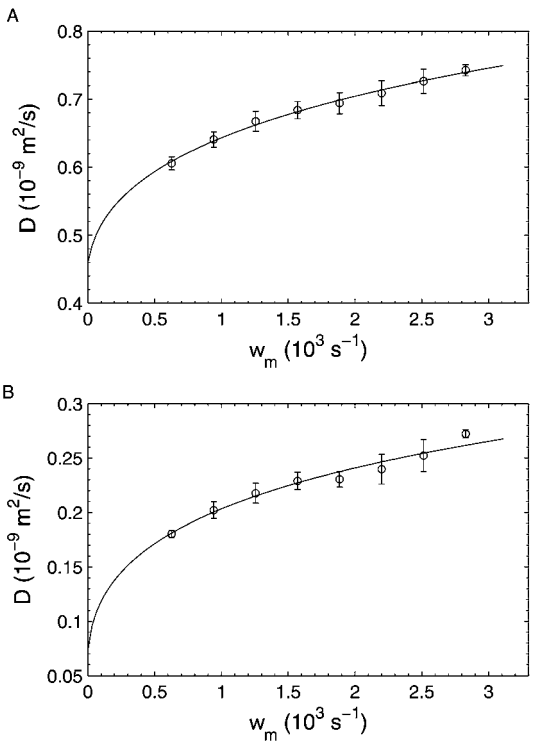

Fig. 5 Diffusion spectrum for water (A) and TMA (B) in the TMA-oleate sample. Theoretical model (solid lines, according to eqn (14)) is fitted to the data (circles). Error bars indicate confidence intervals of 95%.

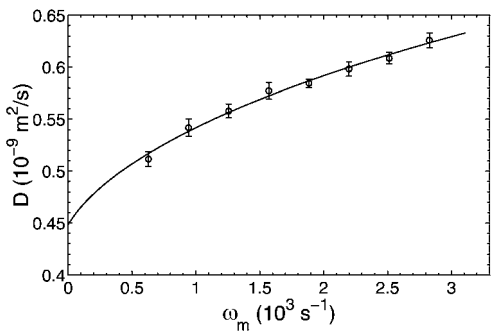

Fig. 6 Diffusion spectrum water in the Na-oleate sample. Theoretical model (solid line) is fitted to the data (circles). Error bars indicate confidence intervals of 95%.

confinements in the nm-range but they do indicate the presence of polydisperse confinements with sizes in the μm-range.

As noted above, the long-time diffusion values obtained for water (see Table 1) are lower by a factor of 2 then the ones predicted in the theory section for a system of densely packed vesicles. However, it should be noted that the vesicles in this systems are densely packed, *i.e.* the hydrated bilayers are in contact and along these contact regions of the vesicles basically no free water is present. The additional barriers on the μm length-scale, as indicated by the λ_{hom} and the $D(\omega)$ measurements, might be responsible for the difference between the measured and the predicted long-range diffusion values.

Combining results presented here with prior results,[5,8–10] suggests a complex structure where both small unilamellar vesicles and large confinements are present. An inhomogeneous sample with spatial variation in the volume fraction of vesicles seems unreasonable on account of the electrostatic interactions that are present between the vesicles. The small vesicles being confined in either bigger vesicles or a bilayer-network is a more reasonable suggestion.

5 Conclusions

The presented NMR diffusion results indicate the presence of confinements on the μm-range in a vesicle gel, composed of small unilamellar vesicles as building blocks. This length-scale is considerably larger than the small unilamellar vesicles which has been shown to be present before.[5] The new results do not contradict former experimental findings, since the NMR measuring techniques are sensitive to different length scales than those previously probed. This is evidenced by the different q-ranges used in the scattering and NMR techniques. Both the scattering and the electron microscopy techniques monitor small structures, down to the nm-range and would not be able to identify the structures on the μm-scale to which the diffusion NMR techniques are sensitive.

A combination of the two NMR techniques presented here (PGSE and MGSE) provides a robust evidence of a complex morphology of the vesicle gels. The results of the two techniques are complementary, consistent, and therefore give strong support in favour of the validity of the structural results obtained. The PGSE experiment offers a fast way of identifying the length scale on which structural features are present in the samples with complex morphology. The MGSE experiment provides additional information on size polydispersity of the confinements.

The "super-structure" in the μm-range of highly ordered vesicle gel systems, is a novel and important finding with respect to a better understanding of these systems. These results are also interesting for a variety of applications of vesicle gels. Such a "super-structure" might be important for a comprehensive understanding not only of their structure but also of the release properties in the case of encapsulated active agents.

6 Acknowledgements

We would like to thank Dr L. Noirez and Dr S. Prevost for help with the SANS experiments.

This work is financially supported by the Swedish Foundation for Strategic Research (SSF) and the Swedish Research Council

(VR) through the Linnaeus Center of Excellence on Organizing Molecular Matter (OMM) along with the Crafoord Foundation.

References

1 D. F. Evans and H. Wennerström, *Colloidal Domain, where Physics, Chemistry, Biology and Technology Meet*, Wiley-VCH, New York, 1999.
2 K. Holmberg, B. Jönsson, B. Kronberg and B. Lindman, *Surfactants and Polymers in Aqueous Solutions*, Wiley-VCH, Chichester, 2nd edn, 2002.
3 Y. Chevalier and T. Zemb, *Rep. Prog. Phys.*, 1990, **53**, 279–371.
4 S. Förster, V. Abetz and A. H. E. Müller, in *Polyelectrolyte Block Copolymer Micelles*, Springer, Berlin, Heidelberg, 2004, vol. 166, pp. 173–210.
5 M. Gradzielski, *J. Phys.: Condens. Matter*, 2003, **15**, R655–R697.
6 H. Hoffmann, C. Thunig, P. Schmiedel and U. Munkert, *Faraday Discuss.*, 1995, **101**, 319–333.
7 H. Hoffmann, C. Thunig, P. Schmiedel and U. Munkert, *Langmuir*, 1994, **10**, 3972–3981.
8 M. Gradzielski, *Curr. Opin. Colloid Interface Sci.*, 2004, **9**, 149–153.
9 M. Gradzielski, M. Müller, M. Bergmeier, H. Hoffmann and E. Hoinkis, *J. Phys. Chem. B*, 1999, **103**, 1416–1424.
10 K. Fontell, L. Mandell and P. Ekwall, *Acta Chem. Scand.*, 1968, **22**, 3209–3223.
11 M. Gradzielski, M. Bergmeier, H. Hoffmann, M. Müller and I. Grillo, *J. Phys. Chem. B*, 2000, **104**, 11594–11597.
12 P. Callaghan, *Principles of Nuclear Magnetic Resonance Spectroscopy*, Oxford Press, Oxford UK, 1991.
13 W. Price, *NMR Studies of Translational Motion: Principles and Applications*, Cambridge University Press, Oxford UK, 2009.
14 J. E. Tanner and E. Stejskal, *J. Chem. Phys.*, 1968, **49**, 1768–1777.
15 J. Kärger and W. Heink, *J. Magn. Reson.*, 1983, **51**, 1–7.
16 P. T. Callaghan, C. D. Eccles and Y. Xia, *J. Phys. E: Sci. Instrum.*, 1988, **21**, 820–822.
17 P. T. Callaghan, D. MacGowan, K. J. Packer and F. O. Zelaya, *J. Magn. Reson.*, 1990, **90**, 177–182.
18 P. Callaghan, A. Coy, D. MacGowan, K. Packer and F. O. Zelaya, *Nature*, 1991, **351**, 467–469.
19 M. H. Blees, *J. Magn. Reson., Ser. A*, 1994, **109**, 203–209.
20 P. Linse and O. Söderman, *J. Magn. Reson., Ser. A*, 1995, **116**, 77–86.
21 C. Malmborg, D. Topgaard and O. Söderman, *J. Magn. Reson.*, 2004, **169**, 85–91.
22 C. Malmborg, M. Sjöbeck, S. Brockstedt, E. Englund, O. Söderman and D. Topgaard, *J. Magn. Reson.*, 2006, **180**, 280–285.
23 I. Åslund and D. Topgaard, *J. Magn. Reson.*, 2009, **201**, 250–254.
24 I. Åslund, C. Cabaleiro-Lago, O. Söderman and D. Topgaard, *J. Phys. Chem. B*, 2008, **112**, 2782–2794.
25 I. Åslund, B. Medrohno, O. Söderman, D. Topgaard and C. Schmidt, Submitted.
26 J. Stepišnik, *Prog. Nucl. Magn. Reson. Spectrosc.*, 1985, 187–209.
27 P. Callaghan and J. Stepišnik, *J. Magn. Reson.,Ser. A*, 1995, **117**, 118–122.
28 P. T. Callaghan and J. Stepišnik, *Adv. Magn. Opt. Reson.*, 1996, **19**, 325–388.
29 J. Stepišnik, *Europhys. Lett.*, 2002, **60**, 453–459.
30 J. Stepišnik, *Phys. B*, 1993, **183**, 343–350.
31 J. Stepišnik, A. Mohorič and A. Duh, *Phys. B*, 2001, **307**, 158–168.
32 J. Stepišnik, S. Lasič, A. Mohorič, I. Serša and A. Sepe, *J. Magn. Reson.*, 2006, **182**, 195–199.
33 S. Lasič, I. Åslund and D. Topgaard, *J. Magn. Reson.*, 2009, **199**, 166–172.
34 D. Topgaard, C. Malmborg and O. Söderman, *J. Magn. Reson.*, 2002, **156**, 195–201.
35 E. O. Stejskal, *J. Chem. Phys.*, 1965, **43**, 3597–3603.
36 D. E. Woessner, *J. Phys. Chem.*, 1963, **67**, 1365–1367.
37 D. S. Grebenkov, *Rev. Mod. Phys.*, 2007, **79**, 1077–1137.
38 W. S. Price and P. W. Kuchel, *J. Magn. Reson.*, 1991, **94**, 133–139.
39 C. S. Johnson, *Prog. Nucl. Magn. Reson. Spectrosc.*, 1999, **34**, 203–256.
40 D. Topgaard and O. Söderman, *Magn. Reson. Imaging*, 2003, **21**, 69–76.
41 R. Kubo, *Lectures in Theoretical Physics*, Interscience Publishers Ltd., London, 1959, vol. 1.
42 J. Stepišnik, *Phys. B*, 1999, **270**, 110–117.
43 A. V. Barzykin, K. Hayamizu, W. S. Price and M. Tachiya, *J. Magn. Reson., Ser. A*, 1995, **114**, 39–46.
44 B. Jönsson, H. Wennerström, P. G. Nilsson and P. Linse, *Colloid Polym. Sci.*, 1986, **264**, 77–88.
45 C. Malmborg, D. Topgaard and O. Söderman, *J. Colloid Interface Sci.*, 2003, **263**, 270–276.
46 J. E. Tanner, *J. Chem. Phys.*, 1970, **525**, 2523–2526.
47 U. Keiderling, *Appl. Phys. A: Mater. Sci. Process.*, 2002, **74**, S1455–S1457.
48 K. J. Packer and C. Rees, *J. Colloid Interface Sci.*, 1972, **40**, 206–218.
49 B. Balinov, O. Urdahl, O. Söderman and J. Sjöblom, *Colloids Surf., A*, 1994, **82**, 173–181.
50 M. L. Johns and K. G. Hollingsworth, *Prog. Nucl. Magn. Reson. Spectrosc.*, 2007, **50**, 51–70.